Bridge vibration measurements from very high-resolution spaceborne SAR

Aleksanteri B. Vattulainen*, Finlay Rollo*, Alessandro Lotti‡, Daniel Tonelli‡, Sebastian Diaz Riofrio*, Enrico Tubaldi†, Daniele Zonta‡, Christos Ilioudis*, Pietro Milillo§ and Carmine Clemente*
*Department of Electronic and Electrical Engineering, University of Strathclyde,
†Department of Civil Engineering, University of Strathclyde,
‡Department of Civil, Environmental and Mechanical Engineering, University of Trento,
§Department of Civil and Environmental Engineering, University of Houston

***Abstract*—Structural health monitoring (SHM) using vibrometry is a key technique for the maintenance of bridges and other infrastructure. Conventional methods require in-situ placement of sensors which can be costly and inconvenient. This paper presents a *remote* monitoring method for extracting vibrational information from very high-resolution SAR data. This was achieved using a combination of a modified back-projection algorithm, spectrogram, and cadence-frequency analysis, which was applied to SAR data of a bridge. The extracted vibrations were validated against synchronous in-situ ground truth measurements.**

***Index Terms*—SAR, micro-Doppler, structural health monitoring**

I. Introduction

Structural health monitoring (SHM) is widely used to assess the condition of bridges and buildings. Vibration-based SHM is a key technique which measures the dynamic behaviour of structures and their modal parameters, such as natural frequencies, damping, and mode-shapes [1]. Monitoring these parameters over time can identify damage or degradation, as changes in stiffness affect the modal properties [2]. Measurement of bridge vibrations is conventionally performed during random ambient excitation with sensors such as linear variable differential transformers (LVDTs) or accelerometers. These devices require in-situ placement which can lead to high costs due to road closures, installation, and maintenance [3].

Different remote sensing approaches have been explored: laser Doppler vibrometers [4] are accurate, but require the installation of a relatively large and expensive device; whereas motion detection cameras [5] are more affordable, but can be vulnerable to picking up vibrations of the sensor (rather than the target) and require sufficient illumination to function.

Radar offers an alternative which is robust in all weather and lighting conditions, where implementations for infrastructure monitoring have been both ground-based, such as interferometric radars [6], and spaceborne, namely synthetic aperture radars (SAR) [7]. A SAR system has the potential to provide the best coverage – the large observed area during a data collection allows simultaneous monitoring of many targets, and as an orbiting sensor, the same satellite can observe structures anywhere along its flight-path. Spaceborne satellites and constellations also provide frequent repeat passes for close monitoring, and archive data can be used to measure past states. Previous work using spaceborne SAR for this application typically used long time-series interferometric data for deformation analysis [8], [7]. More recently, an emerging category of techniques exploits the micro-Doppler (m-D) effect [9] to characterise the vibrations of structures during the period of the acquisition.

The signature of a sinusoidally vibrating target is shown in Eq. 1 [10]:

$$s_{\mathrm{v}}(x,t) = \sigma_{\mathrm{v}} e^{i\frac{4\pi}{\lambda_{\mathrm{c}}}R(x)} e^{i\sin(2\pi f_{\mathrm{v}} t)} \tag{1}$$

as a function of along track position x and time t, σ_{v} and f_{v} are the radar cross section and vibration frequency of the target respectively, $R(x)$ is the slant range and λ_{c} is the carrier wavelength. In SAR, image reconstruction is achieved by compensating for the phase changes due to the platform motion and the varying distance to the *assumed to be static* scene. The phase from target movement is generally uncompensated and manifests as imaging artefacts, such as a displacement of the target from its true position (for constant velocity) or as 'ghost targets' (for vibration as shown in Eq. 1). If the phase modulations induced by movement can be measured, they will yield information on the target motion.

Numerous techniques exist for SAR m-D extraction: in [11], this was treated as a polynomial phase signal estimation problem and was used to measure the vibrational motion of a corner reflector on a dam; in [12] and [13] a sub-pixel offset tracking approach was used to determine the magnitude of vibrations of both dams and bridges.

This work presents a novel technique for SAR m-D extraction starting from new, long-dwell, SAR data and employing a modified back-projection algorithm (BPA) combined with consolidated m-D measurement tools. The method validation, using Umbra [14] data acquired over a suspension bridge and including simultaneous ground truth measurements using accelerometers on the structure, is also a significant novelty.

II. Micro-Doppler Processing Techniques

Micro-Doppler extraction requires the target phase history, where in SAR this necessitates some 2D localisation of the

This research is funded by the European Space Agency under the projects Bridge Monitoring Based on Single Pass SAR Images, EO4Security - Innovative SAR Processing Methodologies For Security Applications - Topic B2: Micro-Doppler Processing, Fondazione CARITRO (grant number 2021.0224) and the Agreement DPC/ReLUIS 2024-2026 (WP6). This work was in part performed at the University of Houston under a contract with the NASA Commercial Smallsat Data Acquisition Program (QKWEF8XLMTT3).

target to reduce clutter interference. An approach to this is the formation of sub-aperture images by focusing subsections of the full acquisition (aperture). This creates a sequence of images containing the target phase history, which is still also spatially localised – albeit with a lower cross-range resolution and signal to clutter ratio (SCR). In this paper we introduce a modified version of the BPA for sub-aperture image formation from unfocused SAR data.

A. Back-projection Algorithm

A BPA image is formed onto an arbitrary, predefined grid, where each pulse's contribution to each pixel is coherently summed after adjusting for the respective time delays and phase shifts. The per pixel response is given by Eq. 2 [15]:

$$I(\vec{r}) = \sum_{n=1}^{N_\mathrm{p}} s_\mathrm{int}(\vec{r}, \tau_n) \tag{2}$$

where N_p is the total number of pulses, $\vec{r}$ is the pixel location, and τ_n is slow-time. The pixel value, $s_\mathrm{int}(\vec{r}, \tau_n)$, is assigned given the time delay between the pixel and antenna locations, and designated s_int as the discretely sampled range bins do not match $\vec{r}$ exactly and so an interpolation step is required.

By modifying this procedure a new signal of interest (SoI) can be generated. Instead of the final summation, the back-projected pulses can instead be concatenated to form a 3D data cube where the new dimension represents the time axis. This is shown in Eq. 3 where $+\!\!+$ represents concatenation.

$$I(\vec{r}) = s_\mathrm{int}(\vec{r}, \tau_1) +\!\!+ s_\mathrm{int}(\vec{r}, \tau_2) +\!\!+ \ldots +\!\!+ s_\mathrm{int}(\vec{r}, \tau_{N_\mathrm{p}}) \tag{3}$$

By selecting a pixel of interest (by either geographical coordinates, or by detection in the fully formed image), e.g. one with a dominant vibrating scatterer, changes in phase of the pixel can be observed as a function of time.

Use of the BPA to form the SoI in this way is beneficial for four main reasons: 1) all well-established m-D techniques [16] [17] are applicable to the SoI without further preprocessing; 2) the method allows highly localised and precise m-D extraction in both time and location; 3) the pulses can be summed in smaller batches before concatenation, increasing SNR but reducing the effective pulse repetition frequency (PRF); 4) the method allows for eventual image formation by summation along the third dimension. The main drawback is the large amount of memory needed to store the final data cube, but the computational time is the same as the standard BPA.

B. Time-frequency Analysis

The primary m-D extraction is performed with the spectrogram function, defined as the square magnitude of the short-time Fourier transform (STFT) shown in Eq. 4 [18]:

$$\chi(\nu, k) = \left| \sum_{n=0}^{N-1} s(n) w(n-k) e^{-j2\pi\nu n/N} \right|^2 \tag{4}$$

for a signal $s(n)$ as a function of n and total length N, a window function w of length k.

The spectrogram output is typically expressed pictorially and shows the changing frequency of the signal over time. Repeating patterns can be measured from the spectrogram by again applying an STFT in the time dimension as shown in Eq. 5, to form a cadence-velocity diagram (CVD) [19].

$$\Delta(\nu, \epsilon) = \left| \sum_{k=0}^{K-1} \chi(\nu, k) e^{-j2\pi k\epsilon/K} \right| \tag{5}$$

where the STFT is calculated over the full signal. The CVD shows the periodicity of the Doppler frequency components, where a Doppler bin can be taken to form a cadence-frequency spectrum (CFS) to show this more succinctly.

C. Micro-Doppler Extraction Algorithm

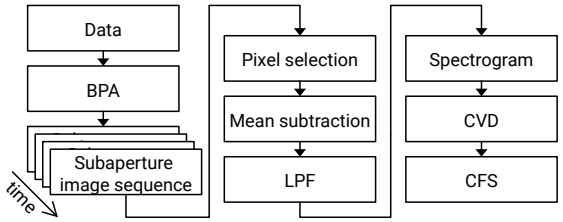

Fig. 1. Algorithm diagram.

The algorithm is shown in Fig. 1, where in summary:

1) The BPA is used to form the sub-aperture images from batches of N_B pulses.
2) A pixel of interest is selected using the focused image.
3) The mean signal level is subtracted from the SoI.
4) The SoI is lowpass filtered (LPF) with a cut-off frequency of f_c.
5) A spectrogram is formed from the SoI using a window size of w and an overlap of $M\%$.
6) A CVD is formed as defined in Eq. 5.
7) The zero Doppler bin of the CVD is extracted to give the CFS.

III. Measurements

The data were collected on 16th May 2024, where the target was the South Portland Street Suspension Bridge in Glasgow, Scotland. This is a 126 m footbridge across the River Clyde as shown in Fig. 2. The SAR data were acquired using the Umbra constellation [14] with the parameters shown in Table I, and supplied in the compensated phase history data (CPHD) format.

Fig. 2. South Portland Street Suspension Bridge (lat.: 55.854937, lon.: −4.255578).

The fully-focused image from this acquisition, processed with the BPA, is shown in Fig. 3. The ground truth measurements were made using 10 single-axis PCB Piezoelectronics Model 393B12 accelerometers [20] in the positions shown in

TABLE I
SAR ACQUISITION AND IMAGE PARAMETERS.

Center frequency	9.6 GHz
PRF / effective PRF	6.06 kHz / 242.4 Hz
Range / azimuth resolution	0.63 m / 0.074 m
Range / azimuth pixel spacing	0.581 m / 0.056 m
Grazing / azimuth angle	41.70° / 101.33°
Slant-range	776.2 km
Platform velocity	7.67 $\mathrm{km\,s^{-1}}$
Dwell-time	22.663 s

Fig. 3. To reconstruct the motion of the bridge, the sensors were paired with one in a vertical orientation and the other in a horizontal orientation, on opposing sides of the bridge as shown in Fig. 3. Accelerometer data acquisitions were then synchronised with the tasked SAR acquisition.

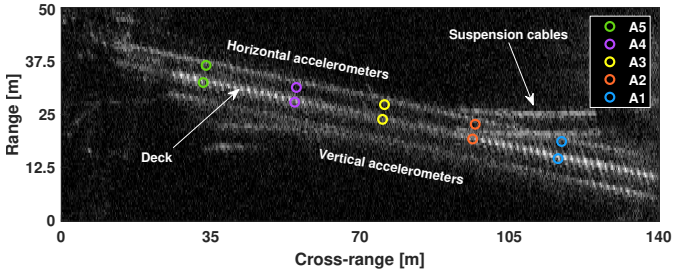

Fig. 3. SAR image of the bridge focused with the BPA, with accelerometer sensor positions overlaid.

A. Ground Truth Projection

The vertical and horizontal ground truth acceleration measurements are combined in the pairs indicated in Fig. 3, and projected onto the radial axis of the radar to give $a_{\mathrm{GT,r}}(t)$. This process is shown in Eqs 6, 7, and 8:

$$a_{\mathrm{V,r}}(t) = -a_{\mathrm{V}}(t)\cos\left(\gamma_{\mathrm{V}} - \gamma_{\mathrm{S}}\right) \tag{6}$$

$$a_{\mathrm{H,r}}(t) = -a_{\mathrm{H}}(t)\cos\left(\phi - \phi_{\mathrm{H}}\right)\cos\left(\gamma_{\mathrm{S}}\right) \tag{7}$$

$$a_{\mathrm{GT,r}}(t) = a_{\mathrm{V,r}}(t) + a_{\mathrm{H,r}}(t) \tag{8}$$

where the variables are defined as: the accelerations a with subscripts V and H to indicate accelerometer orientation, and r to indicate the radial projection; the grazing angles γ with subscripts V and H to indicate the accelerometer orientation and S to denote the satellite grazing angle; and the azimuth angles ϕ with subscripts indicating the value for the horizontal accelerometer and for the satellite. The grazing angle of vertical sensor is by definition 90°. The velocity time-series was calculated by integrating the acceleration history, after which the velocity spectrum was calculated using an FFT.

IV. Results

Processing was conducted using $f_{\mathrm{c}} = 10$ Hz to remove clutter/noise moving at a higher velocity than what is expected from the bridge. The other parameters were set: $N_{\mathrm{B}} = 25$, $w = 50$, and $M = 98\%$. For brevity, the analysis focuses only on measurements from near sensor pair A4, where the velocity spectrum of the bridge at this point is presented together with the SAR estimate in Fig. 4. The spectra were normalised, where first the low frequency spike of the CFS was removed by setting values below 0.3 Hz to zero. The recovered modes are shown in Table II. The ground truth frequency of 1.86 Hz was not detected, and spurious frequencies at approximately 1.3 Hz, 2.30 Hz, and 3.24 Hz were produced by the processing. The peak at 3.24 Hz is a suspected CVD harmonic of the 1.63 Hz mode. In general, the frequency of the modes recovered by the SAR are very good, with more than half of them falling within a single DFT bin width (CFS spacing is 0.045 Hz) of the ground truth. The relative amplitudes of the modes do not match so well, but this is not unexpected. The magnitude of the spectrum from the accelerometers depends on the displacement of the bridge, whilst the CVD measures a cadence whose magnitude depends on the reflectivity of the target.

TABLE II
GROUND TRUTH AND SAR MEASURED MODES.

Sensor pair A4 [Hz]	**SAR** [Hz]	**Absolute error** [Hz]
0.398	0.380	0.018
0.531	0.514	0.017
0.752	0.693	0.059
0.840	0.827	0.013
0.973	0.961	0.012
1.593	1.632	0.039
1.780	1.721	0.059

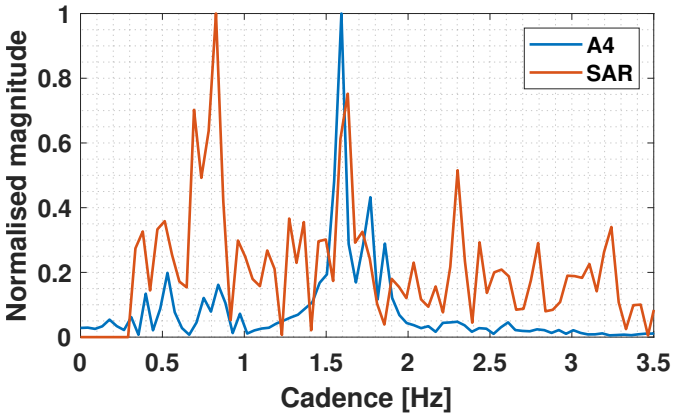

Fig. 4. Vibrational spectrum of the bridge as measured by accelerometer pair A4 and by SAR.

V. Conclusion

A method to extract the vibrational modes of infrastructures from SAR data was presented, based on the BPA and followed by a spectrogram/CFS extraction of the m-D signal modulation. The proposed method was demonstrated to be able to estimate most of the main modes of vibration with good agreement to in-situ measurements, with over half falling within a DFT bin width of the CFS. As future work, incoherent and coherent integration of signal samples will be explored to improve SCR, the frequency extraction will be fully calibrated, and possible methods for calibrating spectrum magnitudes from the CVD explored.

Acknowledgment

We extend our gratitude to Umbra Lab for providing the dataset.

REFERENCES

[1] H. N. Li, L. Ren, Z. G. Jia, T. H. Yi, and D. S. Li, "State-of-the-art in structural health monitoring of large and complex civil infrastructures," *Journal of Civil Structural Health Monitoring*, vol. 6, no. 1, pp. 3–16, 2 2016.

[2] J. M. W. Brownjohn, A. De Stefano, Y.-L. Xu, H. Wenzel, and A. E. Aktan, "Vibration-based monitoring of civil infrastructure: challenges and successes," *Journal of Civil Structural Health Monitoring*, vol. 1, no. 3-4, pp. 79–95, 12 2011.

[3] M. Pozzi and A. Der Kiureghian, "Assessing the value of information for long-term structural health monitoring," in *Health Monitoring of Structural and Biological Systems 2011*, vol. 7984. SPIE, 3 2011, p. 79842W.

[4] H. H. Nassif, M. Gindy, and J. Davis, "Comparison of laser Doppler vibrometer with contact sensors for monitoring bridge deflection and vibration," *NDT & E International*, vol. 38, no. 3, pp. 213–218, 4 2005.

[5] J. J. Lee and M. Shinozuka, "A vision-based system for remote sensing of bridge displacement," *NDT & E International*, vol. 39, no. 5, pp. 425–431, 7 2006.

[6] M. Pieraccini, "Monitoring of Civil Infrastructures by Interferometric Radar: A Review," *The Scientific World Journal*, vol. 2013, pp. 1–8, 2013.

[7] V. Macchiarulo, P. Milillo, C. Blenkinsopp, C. Reale, and G. Giardina, "Multi-temporal InSAR for transport infrastructure monitoring: recent trends and challenges," *Proceedings of the Institution of Civil Engineers - Bridge Engineering*, vol. 176, no. 2, pp. 92–117, 6 2023.

[8] P. Ma, H. Lin, W. Wang, H. Yu, F. Chen, L. Jiang, L. Zhou, Z. Zhang, G. Shi, and J. Wang, "Toward Fine Surveillance: A review of multitemporal interferometric synthetic aperture radar for infrastructure health monitoring," *IEEE Geoscience and Remote Sensing Magazine*, vol. 10, no. 1, pp. 207–230, 3 2022.

[9] V. C. Chen, *The Micro-Doppler Effect in Radar*, 2nd ed. Artech house, 2019.

[10] D. Muff, M. Stevens, D. Blacknell, M. Nottingham, C. Stevenson, and H. Griffiths, "Detecting Vibrating Targets in Fine Resolution SAR Imagery," in *EUSAR 2018; 12th European Conference on Synthetic Aperture Radar*. Aachen, Germany: VDE, 8 2018.

[11] A. Anghel, G. Vasile, C. Ioana, R. Cacoveanu, and S. Ciochina, "Micro-Doppler Reconstruction in Spaceborne SAR Images Using Azimuth TimeFrequency Tracking of the Phase History," *IEEE Geoscience and Remote Sensing Letters*, vol. 13, no. 4, pp. 604–608, 4 2016.

[12] F. Biondi, P. Addabbo, C. Clemente, S. L. Ullo, and D. Orlando, "Monitoring of Critical Infrastructures by Micromotion Estimation: The Mosul Dam Destabilization," *IEEE Journal of Selected Topics in Applied Earth Observations and Remote Sensing*, vol. 13, pp. 6337–6351, 2020.

[13] F. Biondi, P. Addabbo, S. L. Ullo, C. Clemente, and D. Orlando, "Perspectives on the Structural Health Monitoring of Bridges by Synthetic Aperture Radar," *Remote Sensing*, vol. 12, no. 23, p. 3852, 11 2020.

[14] "Delivering Global Omniscience Umbra Space." [Online]. Available: https://umbra.space/

[15] L. A. Gorham and L. J. Moore, "SAR image formation toolbox for MATLAB," in *Algorithms for Synthetic Aperture Radar Imagery XVII*, vol. 7699. SPIE, 4 2010, p. 769906.

[16] C. Clemente, A. Balleri, K. Woodbridge, and J. J. Soraghan, "Developments in target micro-Doppler signatures analysis: radar imaging, ultrasound and through-the-wall radar," *EURASIP Journal on Advances in Signal Processing*, vol. 2013, no. 1, p. 47, 12 2013.

[17] F. Fioranelli, H. Griffiths, M. Ritchie, and A. Balleri, *Micro-Doppler Radar and Its Applications*, F. Fioranelli, H. Griffiths, M. Ritchie, and A. Balleri, Eds. Institution of Engineering and Technology, 7 2020.

[18] R. I. A. Harmanny, J. J. M. de Wit, and G. P. Cabic, "Radar micro-Doppler feature extraction using the spectrogram and the cepstrogram," in *2014 11th European Radar Conference*. IEEE, 10 2014, pp. 165–168.

[19] S. Bjorklund, T. Johansson, and H. Petersson, "Evaluation of a micro-Doppler classification method on mm-wave data," in *2012 IEEE Radar Conference*. IEEE, 5 2012, pp. 0934–0939.

[20] "Model 393B12 | PCB Piezotronics." [Online]. Available: https://www.pcb.com/products?m=393b12